



POLITECNICO
MILANO 1863

SCUOLA DI INGEGNERIA INDUSTRIALE
E DELL'INFORMAZIONE

EXECUTIVE SUMMARY OF THE THESIS

Multicopter UAV control via dynamic inversion

LAUREA MAGISTRALE IN AEROSPACE ENGINEERING - INGEGNERIA AEROSPAZIALE

Author: SOUFIANE EL OMARI

Advisor: PROF. MARCO LOVERA

Co-advisor: GIOVANNI GOZZINI

Academic year: 2023-24

1. Introduction

This thesis covers the design, implementation, and analysis of a dynamic inversion based controller on a small scale drone. Quadrotors have gained significant popularity in recent years for their ease of use and numerous applications such as environment monitoring and surveillance. The control aspect of quadrotors is of particular importance due to the absence of a pilot. This work aims at studying an innovative methodology for control of quadrotors.

The first part of the project includes a modeling and system identification campaign of the quadrotor. The models were derived beginning from the equations of motion with certain assumptions for simplicity. A grey-box estimation was used based on the output-error method covering the longitudinal, lateral, directional, and vertical dynamics of the drone.

The identified plant was used to design a dynamic inversion controller architecture, leveraging the dynamics of the system. This part included the formulation and simulation in both Simulink and Software-In-The-Loop (SITL), which provided an understanding of the system behavior and tuning of controller parameters. Flight tests were performed once the controller was ready at the FlyART laboratory of

Politecnico di Milano.

To assess the stability concerns of the dynamic inversion methodology, a comprehensive look at the robust stability of the controller was performed. The analysis included classic methods such as frequency analysis and Monte Carlo approach, as well as robust techniques in structured singular value analysis.

2. Experimental Setup

The work presented in this thesis was carried out at the FlyART laboratory of Politecnico di Milano. This laboratory hosts many research activities for drones and other flying objects in its arena. The drone used for this setup is the ANT-X shown in Figure 1. The drone can be operated wirelessly through a ground control system and is equipped with the necessary devices for reading, communication, and computation. The flight baseline autopilot of the ANT-X features a cascade architecture which was used to perform the identification experiments. The simulations were performed on Simulink and a Software-In-The-Loop simulator designed by ANT-X for the drone platform.

3. Grey-box identification

To design and implement the dynamic inversion based controller, a structured model of the drone was necessary. For this reason, a system identification campaign was carried out on the ANT-X. The model used is derived from the equations of motion of the UAV which were linearized and decoupled under low-speed assumption. The complete model features longitudinal, lateral, directional, and vertical dynamics which are the necessary for successfully controlling these types of quadrotors. Results are reported for each model, the verification of the quality of the estimate was done computing the variance accounted for between the identified model and validation data [1], as well as the normalized root mean square error as a measure of the fit.

3.1. Longitudinal model

The longitudinal model was identified using a frequency domain approach starting from its response to a long duration quadratic sweep signal. The choice of input signal was carefully studied [2] as the longitudinal and lateral dynamics are unstable and required testing in closed loop. The linear longitudinal system is:

$$\begin{bmatrix} \dot{u} \\ \dot{q} \\ \dot{\theta} \end{bmatrix} = \begin{bmatrix} X_u & X_q & -g \\ M_u & M_q & 0 \\ 0 & 1 & 0 \end{bmatrix} \begin{bmatrix} u \\ q \\ \theta \end{bmatrix} + \begin{bmatrix} X_\delta \\ M_\delta \\ 0 \end{bmatrix} \delta_{long}$$

Where the vector of unknown parameters contain the stability derivatives (X_u, X_q, M_u, M_q) and the control derivatives (X_δ, M_δ). u is the longitudinal velocity in the body frame, a_x is the longitudinal acceleration defined in the body frame, q the pitch rate defined in rad/s , and θ is the pitch angle defined in rad . The results of the identification are reported in Table 1:

Parameter	Value	$\sigma\%$
X_u	-0.1015/s	21.448
X_q	-0.043954m/srad	18.86
X_δ	6.8626 m/s ²	5.7967
M_u	3.191rads/m	7.8898
M_q	0.72024/s	13.919
M_δ	574.61rad/s ²	0.99916

Table 1: Longitudinal model estimated parameters and standard deviation

The model showed good fit with respect to validation data and the uncertainty was not exceedingly high.

3.2. Lateral model

Similar to the longitudinal model, a frequency domain approach was considered for the lateral identification. The same injection sweep signal was used and the model is defined as follows:

$$\begin{bmatrix} \dot{v} \\ \dot{p} \\ \dot{\phi} \end{bmatrix} = \begin{bmatrix} Y_v & Y_p & g \\ L_v & L_p & 0 \\ 0 & 1 & 0 \end{bmatrix} \begin{bmatrix} v \\ p \\ \phi \end{bmatrix} + \begin{bmatrix} Y_\delta \\ L_\delta \\ 0 \end{bmatrix} \delta_{lat}$$

Where the vector of unknown parameters contain the stability derivatives (Y_v, Y_p, L_v, L_p) and the control derivatives (Y_δ, L_δ). v is the lateral velocity in the body frame, a_y is the lateral acceleration defined in the body frame, p the roll rate defined in rad/s , and ϕ is the roll angle defined in rad . The results are shown in Table 2:

Parameter	Value	$\sigma\%$
Y_v	-0.27567/s	15.543
Y_p	0.01639 m/(srad)	90.737
Y_δ	-2.645 m/s ²	16.391
L_v	3.7846rads/m	9.1561
L_p	1.1364/s	10.333
L_δ	686.6rad/s ²	0.81786

Table 2: Lateral model estimated parameters and standard deviation

The lateral dynamics showed high standard deviation of the stability derivative for the roll rate Y_p , the parameter was excluded from the model and assumed equal to zero. The nominal model showed good fit with respect to validation data.

3.3. Vertical and directional dynamics

The vertical and directional dynamics were inherently stable and both used a time domain identification starting from the response to a PRBS signal. The VAF and NRMSE of the results were good and the estimated parameters had low standard deviations.

The directional model and results are reported below, Where the vector of unknown parameters contain the stability derivative N_r and the control derivative N_δ . r is the yaw rate in rad/s , ψ is the yaw angle in rad :

$$\begin{bmatrix} \dot{r} \\ \dot{\psi} \end{bmatrix} = \begin{bmatrix} N_r & 0 \\ 1 & 0 \end{bmatrix} \begin{bmatrix} r \\ \psi \end{bmatrix} + \begin{bmatrix} N_\delta \\ 0 \end{bmatrix} \delta_{dir} \quad (1)$$

The vertical model and results are reported below, Where the vector of unknown parameters

Parameter	Value	$\sigma\%$
N_r	-17.981/s	3.1124
N_d	257.06rad/s ²	1.7156

Table 3: Directional model estimated parameters and standard deviation

contain the stability derivative Z_w and the control derivative Z_d , where ω is the vertical velocity:

$$\dot{w} = Z_w w + Z_d \delta_{\text{vert}} \quad (2)$$

Parameter	Value	$\sigma\%$
Z_w	-0.615141/s	1.9633
Z_d	-23.748m/s ²	0.3948

Table 4: Vertical model estimated parameters and standard deviation

4. Dynamic inversion controller design

A controller based on dynamic inversion was designed to achieve stability and disturbance rejection. The controller featured an inner loop for attitude and vertical velocity tracking and an outer loop for longitudinal and lateral velocities. The design follows this methodology [3]: Let us consider a MIMO system with state variable $x(t) \in R^n$, input $u(t) \in R^m$ and output $y(t) \in R^p$. We can then write the system update and readout equations as follows:

$$\dot{x} = Ax + Bu \quad (3)$$

$$y = Cx \quad (4)$$

For the purposes of the analysis, the matrix D is omitted. Note that the inversion can be done for any system with $A \in R^{n \times n}$, $B \in R^{n \times m}$ and $C \in R^{p \times n}$. Next, we differentiate the output equation until the explicit dependence of control input $\mathbf{u}(\mathbf{t})$ is seen:

$$\dot{y} = CAx + CBu \quad (5)$$

The equation is then inverted to express the input needed to drive an output in y :

$$u = (CB)^{-1}(v - CAx) \quad (6)$$

$$v = \dot{y}_{cmd_f} + Ke \quad (7)$$

$$e = y_{cmd_f} - y \quad (8)$$

where v is the pseudo command vector and K is the compensator of e , which is the difference between the filtered desired output y_{cmd_f} and the measured output y .

The dynamic inversion also features filter blocks to smoothen the input and allow for better tracking.

4.1. Simulink model

The flight controller was modeled in Simulink and simulated using the complete model, which includes all the dynamics in a block diagonal configuration. This simulation allowed for testing the controller and obtaining a preliminary tuning for the PID and PI parameters. The controller was able to stabilize the unstable longitudinal and lateral dynamics and provided good tracking and accuracy.

4.2. Software In the Loop

A software in the loop simulator [4] was used primarily to test and troubleshoot the controller implementation of the complete auto-pilot architecture including the actuator model and communication protocols. The SITL behaves similarly to the real drone as it uses the same framework of the flight control unit onboard the ANT-X. This allows for ease of troubleshooting and testing of the actuator model. The SITL model is designed in a 3D software by Open Robotics named Gazebo. Since the models are different, adjustments to the controller were made and comparison with the Simulink results are reported in Figures 2 and 3 for the longitudinal and lateral dynamics respectively. The SITL simulation highlighted an important issue with yaw dynamic model, which proved to be unstable (Figure 5). The vertical dynamics also showed some difficulty with compensating the gravity effects as shown in Figure 4 which was rectified. Further tuning was performed obtaining the results seen in Figure 6 for the yaw dynamics with the final controller data are reported in Table 5.

4.3. Flight test results

With the controller architecture and parameters ready, a flight test was performed on the ANT-X at the FlyART arena. The input for the velocities in all direction was a doublet of 0.5 m/s. The yaw dynamics was tested using a doublet in yaw

Gains	K_P	K_I	K_D
Roll angle	136	200	20
Pitch angle	136	200	20
Longitudinal velocity	1.8	1	-
Lateral velocity	1.8	1	-
Vertical velocity	1.8	1	-
Yaw rate	45	625	-

Table 5: Tuned controller parameters

angle of 30 deg. The results of the flight experiment are reported in Figures 7, 8, 9, and 10. The longitudinal, vertical, and directional dynamics all performed well with very good tracking and little overshoot. The modifications to the yaw and vertical velocity models was able to ameliorate the system response. The lateral dynamics showed slight error in tracking, which is due to the small difference in the identified model with respect to the longitudinal one.

5. Robust stability analysis

As discussed previously, dynamic inversion is highly susceptible to uncertainty on the parameters and model quality, as it assumes perfect knowledge of the model variables. This highlights the importance of designing a robustly stable controller, able to handle the uncertainty stemming from identification errors. For this analysis, the inner loop attitude controller is considered with the standard deviations of the parameters defined in the identification process.

5.1. Uncertainty analysis

An uncertainty analysis on the inner loop was performed studying the behavior of the open loop system. The inversion creates a marginally stable dynamic similar to an integrator. The standard deviation defined in Gaussian distribution drives the poles of the system to the stable or unstable region, which is highly undesirable. In closed loop however, the controller is able to stabilize the dynamics both nominally and in the presence of uncertainty.

5.2. LFT and structured singular value analysis

To study the effects uncertainty using more robust methods, a SSV analysis was performed. First the system was transformed into the M- Δ form [5], which is an LFT form often used in robust stability and analysis techniques. The

SSV provides bounds indicating the worst-case scenario for the system's performance under the designated uncertainties.

- If $\mu \leq 1$, there is no uncertainty $\delta \in \Delta$ that produces a singularity
- If $\mu \geq 1$, there exists an uncertainty $\delta \in \Delta$ that produces a singularity, meaning that the system is not robustly stable to all sets of uncertainty.

From Figure 11 we can see that the controller is able to handle the parametric uncertainty.

5.3. Gap metric and Monte Carlo experiment

Lastly, two iterative methods were performed to simulate the system in the presence of perturbations. The first one is the gap metric [6], which is a measure of how close a system $G_1(s)$ is to system $G_2(s)$ in terms of controllability. In other words it provides a measure of whether the same controller can stabilize both systems. The second method is the Monte Carlo approach, which was used to simulate a range of perturbed systems and analyse their response to check whether the model can shift to the unstable region. Both experiments used a set of 1000 simulations. The system was able to handle all uncertainty with more noticeable sensitivity on the yaw dynamics.

6. Conclusion

To summarize, the grey-box identification of a quadrotor was performed starting from a derived mathematical model. The identified plant of the drone was used to design and fly test an innovative controller based on dynamic inversion techniques with good results in tracking and stability. The uncertainty concerns of the method were addressed in a robust stability analysis, encompassing the inner attitude and vertical models of the drone.

An important finding is the instability in yaw which was not detected using the nominal model simulation. This highlights the importance of using different techniques for troubleshooting and analysis which was taken into consideration moving into the robust stability part.

Further consideration can be discussed in the tuning and identification process. The controller parameter could be improved and other tuning methods considered. The lateral dynamics es-

timates could be enhanced and more research performed on the quality of input/output signals used for the identification. This would allow to push the controller performance capabilities and design it for specific mission profiles or maneuvers.

7. Acknowledgements

My work and passion are dedicated to my mother, who stood by my side and supported me throughout my academic and endeavors. Her belief is my source of my motivation. I wish her a long lasting happy life.

References

- [1] I. Houtzager, J. van Wingerden, and M. Verhaegen, "Fast-array recursive closed-loop subspace model identification," 2009, in Proceedings of the 15th IFAC conference on system identification (SYSID 2009).
- [2] M. Wu and M. Lovera, "Time domain vs frequency domain identification for a small scale helicopter," *CEAS Conference on Guidance, Navigation and Control*, no. 5, 2019.
- [3] U. Saetti, T. Berger, J. Horn, C. Lagoa, and S. Lakhmani, "Design of dynamic inversion and explicit model following control laws for quadrotor inner and outer loops," 05 2018.
- [4] P. Autopilot. Sitl. [Online]. Available: https://docs.px4.io/main/en/sim_gazebo_classic/
- [5] K. Zhou and J. C. Doyle, *Essentials of Robust Control*. Prentice-Hall, 1998.
- [6] D. Fasiku and O. Taiwo, "The use of gap metric analysis in the effective control system design for plants with recycle," *IFAC-PapersOnLine*, vol. 54, no. 21, pp. 186–191, 2021, control Conference Africa CCA 2021.

Figures



Figure 1: ANT-X Drone

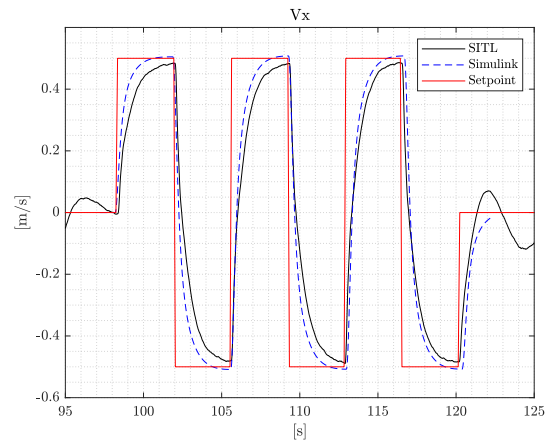


Figure 2: Longitudinal velocity simulated response (SITL against Simulink)

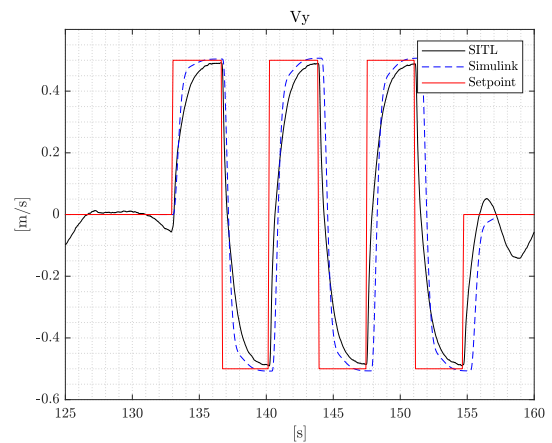


Figure 3: Lateral velocity simulated response (SITL against Simulink)

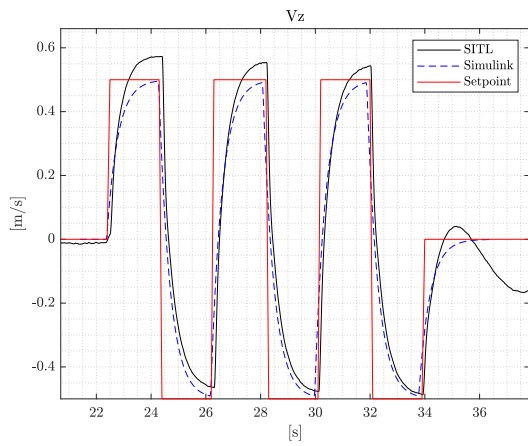


Figure 4: Vertical velocity simulated response (SITL against Simulink)

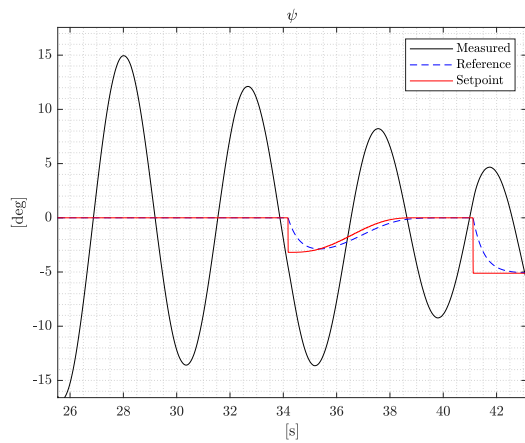


Figure 5: Yaw doublet simulated response (SITL)

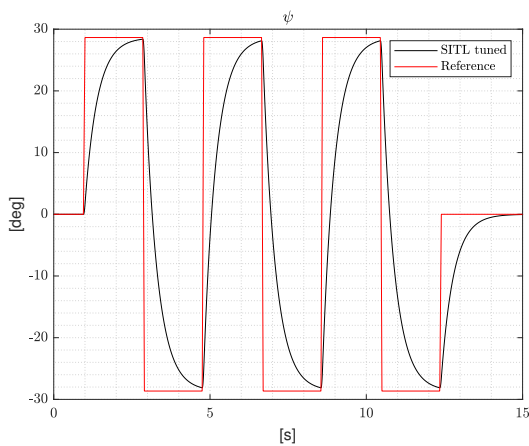


Figure 6: Tuned yaw response (SITL)

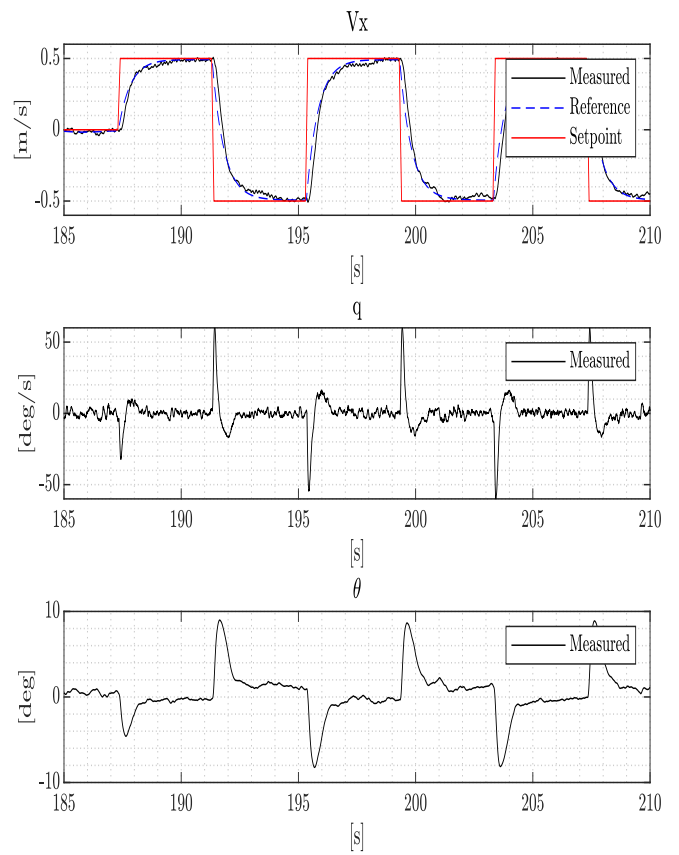


Figure 7: Longitudinal dynamics flight test results

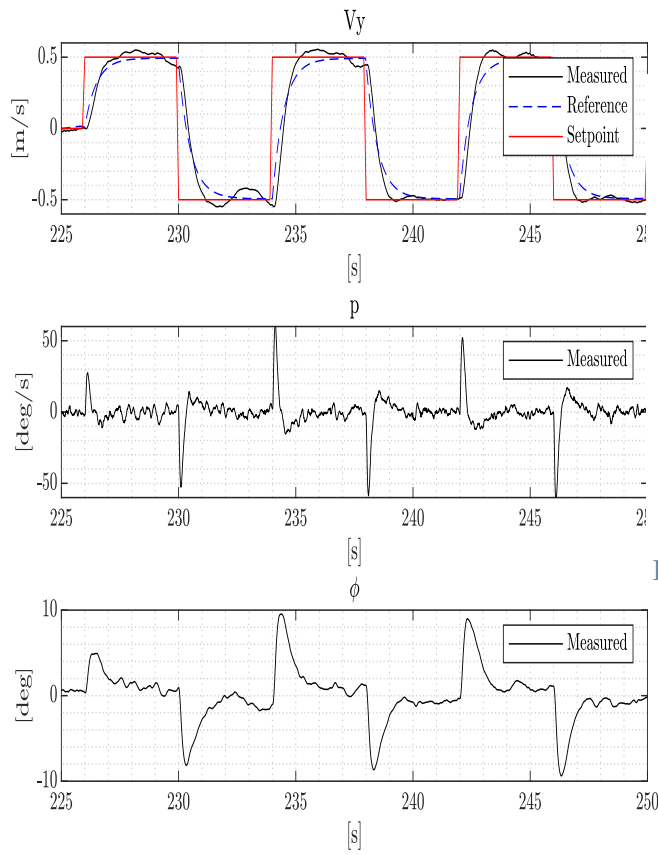


Figure 8: Lateral dynamics flight test results

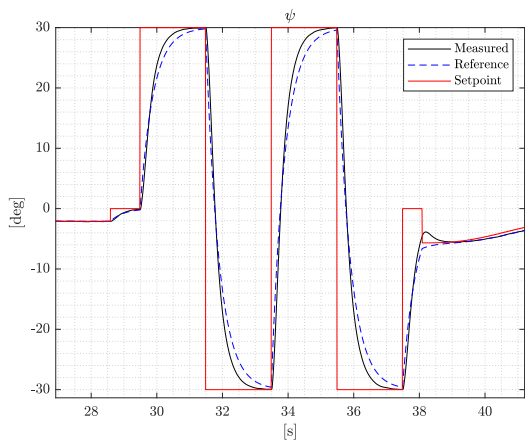


Figure 9: Directional dynamics flight test results

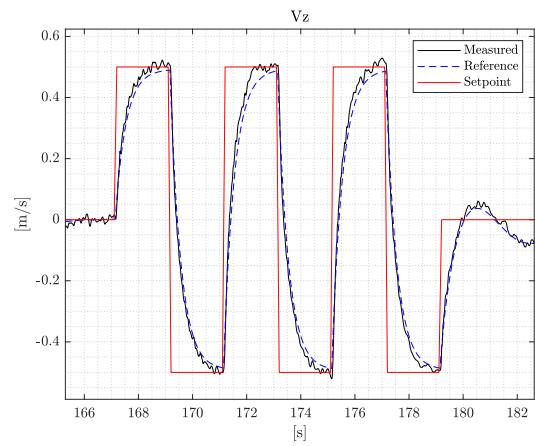


Figure 10: Vertical dynamics flight test results

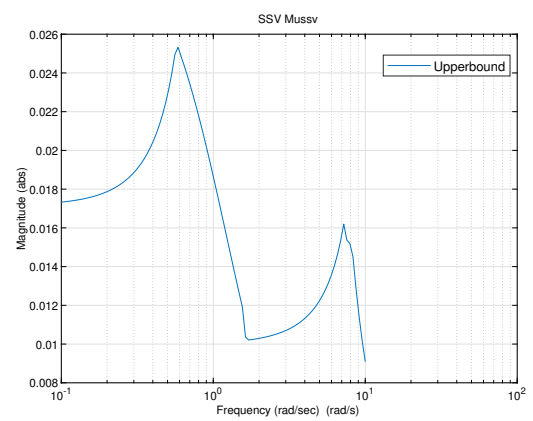


Figure 11: Structured singular value upper bounds